Acoustic Pulse Echoes Probed with Time-Resolved X-Ray Triple-Crystal Diffractometry

Yujiro Hayashi,[1,2] Yoshihito Tanaka,[2,3] Tomoyuki Kirimura,[2] Noboru Tsukuda,[4] Eiichi Kuramoto,[4] and Tetsuya Ishikawa[2]

[1]*Interdisciplinary Graduate School of Engineering Sciences, Kyushu Univ., Kasuga, Fukuoka 816-8580, Japan*
[2]*RIKEN SPring-8 Center, Sayo-cho Sayo-gun, Hyogo 679-5148, Japan*
[3]*CREST, JST, Japan*
[4]*Research Institute for Applied Mechanics, Kyushu Univ., Kasuga, Fukuoka 816-8580, Japan*

Acoustic pulse echoes generated by femtosecond laser irradiation were detected using time-resolved x-ray triple-crystal diffractometry. The determined time-dependent longitudinal strain component for pulse echoes in silicon and gallium arsenide plates showed that the polarity of the strain pulse was dependent on the optically induced initial stress, and that the bipolar pulse waveform was gradually deformed and broadened in the course of propagation. The three-dimensional wave front distortion of pulse echoes was shown simply as the pulse duration broadening, which was consistent with a boundary roughness for an unpolished plate.

Since acoustic wave packets propagating in solid materials produced by ultrashort laser irradiation on the surface were discovered in the 1980s [1], the phenomenon has been investigated intensively [2–4]. The optically induced acoustic pulse echo technique has enabled investigation of underlying structures in materials such as thin layers and defects, as if sonar can detect underwater objects [5–7]. The acoustic pulse echoes have been detected mainly by optical pump-probe methods for polycrystalline metal films with high optical reflectivity. X-ray diffraction (XRD), directly detecting the lattice strain itself regardless of surface condition, is a complementary candidate to the optical probes for acoustic pulse echoes in crystals. However, few XRD methods have been employed for determining the time-dependent strain until recently because of the lack of pulsed and brilliant x-ray sources. Significant progress has been made in the development of such sources: third-generation synchrotron radiation sources or laser-plasma x-ray sources, which have offered time-resolved measurements for acoustic pulses with picosecond resolution [8,9]. The time-resolved XRD (TRXRD) techniques have been applied to the observation of acoustic pulses propagated in highly perfect single crystals of semiconductor in the depth direction [10,11]. While acoustic pulses traveling short distance compared with the transverse size of the laser beam can be considered uniaxial and planar, pulse echoes with three-dimensionally distorted wave fronts due to scattering by defects and complicated boundary structure cannot be described by such ideal one-dimensional plane wave models.

In this Letter, we show a TRXRD method applicable to observation of acoustic pulse echoes: The surface-normal longitudinal component of a strain tensor is determined and the pulse echo waveforms are analyzed considering the three-dimensional distortion effect as the phase deviations of one-dimensional elementary waves. In order to determine the longitudinal strain component in distinction from

the shear components, we employed time-resolved triple-crystal diffractometry (TRTCD) [12], the details of which were reported elsewhere [13]. Since the TRTCD requires more brilliant x-ray sources because of the low efficiency of crystal diffraction, we carried out the measurements at the 27 m long undulator beamline (BL19LXU) of SPring-8, which delivers the brightest x-rays in the world at the moment [14]. The method was examined for the acoustic pulses in typical semiconductors, silicon and gallium arsenide, which are subjected to optically induced electronic stresses with the opposite signs. The temporal change in the pulse waveform due to propagation is observed by detecting each multireflected pulse in the semiconductor plates. As an application, we show the noncontact detection of the surface roughness on the other side to the laser and x-ray irradiation.

The mechanism of acoustic pulse generation due to ultrashort laser irradiation in semiconductors is summarized here [15–17]. When photons with energy E excite electron-hole pairs having excess energy $E_{ex} = E - E_g$ in semiconductors, an electronic stress $-BN\Xi$ is produced if isotropic media are assumed, where N is excess carrier density, $\Xi = \partial E_g / \partial p$, E_g is band gap, p is pressure, and B is bulk modulus. The excess energy is released as thermal energy within 1 ps, which gives rise to a thermal stress $-3B\beta E_{ex}N/C$, where β is linear thermal expansion coefficient and C is specific heat per unit volume. If the optical excitation is impulsive compared with sound propagation, the instantaneous stresses generate a strain pulse forming regions of both dilation and contraction. Assuming that the stresses only depend on depth z, the strain pulse traveling by sound velocity v is expressed by $\epsilon(\eta) \propto (B\Xi/E + 3B\beta E_{ex}/CE)F(\eta)$, where $\eta = z - vt$ and $F(\eta)$ is a waveform function which has been analytically given by bipolar pulse waveforms with the pulse duration of the optical absorption length. The equation predicts that the strain pulses with the opposite polarity are generated depending

on the sign of Ξ, since the second term is negligible. Si and GaAs are the typical semiconductors with negative and positive Ξ, giving rise to the contractional and dilational electronic stress, respectively.

High-purity undoped crystal wafers of Si and GaAs were used to minimize acoustic scattering by defects and impurities. The Si wafer had (111)-oriented surfaces and $h = 1$ mm thickness. For GaAs, two (100)-oriented wafers were sliced from a liquid encapsulated Czochralski ingot to investigate the effect of a rough boundary for pulse echo waveform. While the one GaAs wafer of $h = 600$ μm had the front and back surfaces finished by lapping and then polishing, the other GaAs wafer of $h = 625$ μm had the rough back surface finished by only lapping without polishing. The front surfaces of Si, polished GaAs, and unpolished GaAs wafers were irradiated by laser beam from a mode-locked Ti:sapphire laser with a regenerative amplifier to give rise to the instantaneous electronic stresses. The laser photon energy is $E = 1.55$ eV, which is larger than the band gaps $E_g = 1.11$ and 1.43 eV of Si and GaAs. The pulse duration, fluence, repetition rate, and beam diameter of the laser light were 130 fs full width at half maximum (FWHM), 300 μJ pulse^{-1}, 1 kHz, and $\sim$1 mm, respectively.

The triple-crystal diffractometer was set up using a highly collimated x-ray beam and highly perfect Si crystals for a double-crystal monochromator and an analyzer to detect slight strain as shown in Fig. 1. The monochromatized x rays were incident to the laser-irradiated point on the front surface of the samples through a slit of 40×100 μm^2. To match the optical absorption length 10.6 and 0.75 μm in Si and GaAs with x-ray extinction length, the reflection indices of the samples were chosen to be 333 and 400 for Si and GaAs. The tunability of x-ray energy allowed us to fix the position of the analyzer. Namely, the x-ray photon energy was tuned to 21.9 and 16.2 keV for Si and GaAs, so that the Bragg angle is the same ($\theta_B = 15.7°$). The reflections from the samples were detected by a Si avalanche photodiode (APD) through the analyzer. The angle ω of the sample and θ of the analyzer were controlled with high-precision goniometers [18]. The ω-2θ scan parallel to the reciprocal lattice vector reveals the longitudinal lattice strain component $\Delta d/d$ normal to the surface.

The time-resolved measurement for the ω-2θ scan was conducted by a multichannel scaling technique with a wide time range and a pump-probe method with a higher time
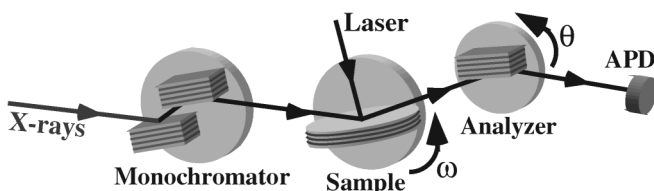
resolution. In the former, the x-ray photons were counted as a function of time with the time interval of 0.8 ns by a multichannel scaler (9353, ORTEC), using trigger pulses from an APD detecting laser pulses. In the latter, the laser timing was controlled by phase lock circuits with respect to an electron bunch in the storage ring with the precision of a few picoseconds, which gave the profile snap shots with the time resolution of the x-ray pulse duration (40 ps FWHM) [19].

The TRXRD profiles in the wide time range were obtained by the multichannel scaling for several angles in the ω-2θ scan. The time-dependent angular shifts of the TRXRD profiles, determined by angular Gaussian fits, are shown in Fig. 2(a) for the Si wafer and in Fig. 2(b) for the polished GaAs wafer. The moment when the peak angles jump due to the laser irradiation is defined as $t = 0$. In the case of the Si wafer, the profile shifts towards the larger angle at $t = 0$ and towards the smaller angle at $t = 162$ ns as shown in the left inset of Fig. 2(a). The profile abruptly shifts to the smaller angle at $t = 215$ ns as shown in the right inset of Fig. 2(a). The abrupt shifts occurring at regular time intervals result from multireflected pulse echoes, since the time interval agrees with the round trip time of an acoustic pulse with the longitudinal sound velocity [20]. The profile shift was determined with the precision of $\sim$0.01 arcsec, corresponding to the measurement accuracy of $\sim 1 \times 10^{-7}$ for the longitudinal strain. In the case of the GaAs wafer, the profile shifts to the smaller angle at $t = 0$, followed by the relaxation, as shown in the left inset of Fig. 2(b). Correspondingly, the profile for the first echo in
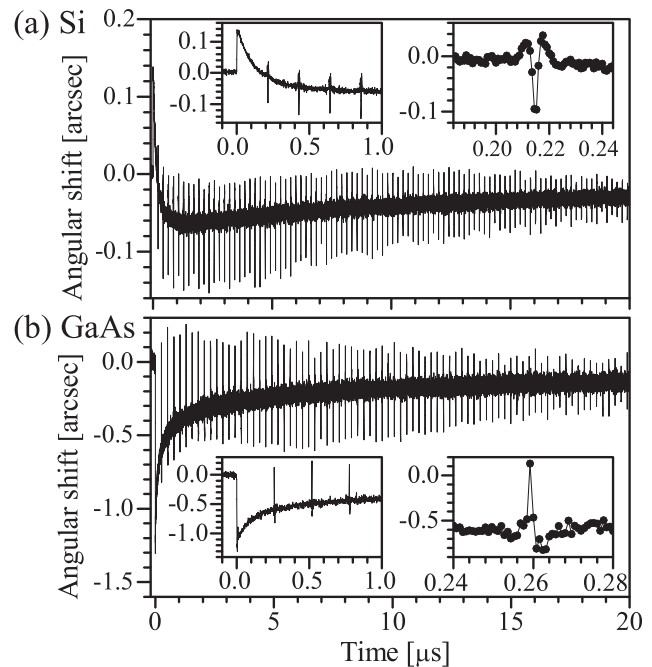
FIG. 2. The angular shift of the TRXRD profile for the Si (a) and the polished GaAs (b) plates irradiated by ultrashort laser pulses. Insets: the regions around the initial shift (left) and the 1st pulse echo (right).

FIG. 1. A schematic illustration of the experimental setup.

the GaAs wafer shifts towards the opposite angle to that of the Si wafer as shown in the right inset of Fig. 2(b).

The experimental results are qualitatively explained by considering that dilation and contraction cause the profile shift to the smaller and larger angle, respectively. In Si, the electronic stress has the opposite sign to the thermal stress, and the magnitude of the contractional electronic stress is 7 times as much as that of the dilational thermal stress under designated values [20]. The following acoustic strain pulse forms dilation-leading bipolar pulse. The initial contraction turns to dilation due to the recombination of the optically induced carriers. Since the acoustic pulse experiences a π phase shift at the back surface with no stress, the contraction-leading bipolar pulse returns to the front surface. As the contraction-leading bipolar pulse echo approaches the front surface, the profile shifts to the larger angle as shown at $t = 209$–213 ns in the right inset of Fig. 2(a). Then the dilation grows when the zero cross point of the bipolar pulse reaches to the front surface, since the dilational tail of the incident pulse is intensified by the dilational lead of reflected pulse. This leads to the strong shift towards the smaller angle at $t = 215$ ns. The contraction tail of the reflected pulse appears at $t = 217$–221 ns, which causes the profile shift to the larger angle. For the GaAs wafer, the dilational electronic and thermal stresses generate the contraction-leading bipolar strain pulse, which results in the opposite process for the pulse echoes to the Si wafer. The above consideration leads us to a conclusion that the behavior of the time-dependent angular shift is similar to that of the temporal derivative of the pulse echo waveform, when the reflection of an echo at a free-end surface is monitored by TRXRD with an extinction depth smaller than the pulse duration.

Observation of the following echoes in GaAs reveals the change in pulse echo shape as time increases. The parts of the 1st, 20th, and 60th echo in Fig. 2(b) are shown in Figs. 3(a)–3(c) by solid circles, respectively, where small open circles in Fig. 3(a) show the result for the 1st echo by the pump-probe method. Compared with the abrupt shift in the 1st echo, the changes in the 20th and 60th echoes are temporally broadened and attenuated. It is seen in the 20th echo part that the profile shift to the small angle after the shift to the large angle grows. The magnitude of the shift to the small angle becomes larger than that to the large angle in the 60th echo part. Considering that the pulse echoes travel several tens of millimeters longer than the diameter of the laser beam, the changes appear to result from the spherical nature of the acoustic pulse. In fact, it is shown that such long-distance propagation gives rise to the deformation of the acoustic pulse waveform by the acoustic diffraction effect [21]. Here, we deal with the three-dimensional wave front distortion of the pulse echo due to scatterers such as boundaries, impurities, defects, and phonons as the one-dimensional superposition of the phase-deviated elementary waves. Since the effect appears as the broadening of the pulse duration assuming the phase deviation with a Gaussian distribution, the TRXRD pro-
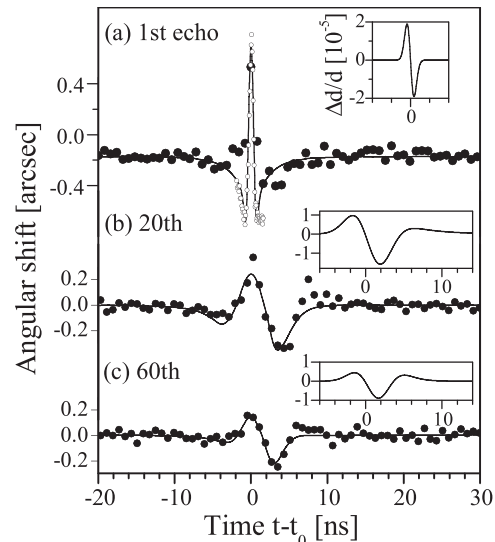
FIG. 3. The angular shift of the TRXRD profile in the part of (a) the 1st, (b) 20th, and (c) 60th pulse echo for the polished GaAs plate with simulation curves. The solid and small open circles show the results by the multichannel scaling and the pump-probe method. The time when the profile reaches the largest angle for each echoes is defined as t_0, where $t_0 = 259.2$, 5169, and 15507 ns for the 1st, 20th, and 60th echo, respectively. Insets: the calculated surface-normal longitudinal strain component for the echoes.

files were calculated by the least square fit of the pulse duration for the waveform function [21]. The calculation was conducted based on the dynamical diffraction theory in the presence of strain, given by Takagi [22] and Taupin [23]. The Takagi-Taupin equation has been solved for one-dimensional strain in the surface-normal direction [24]. The strain profile formed when the acoustic pulse reflects at a free boundary was used. The angular shift of the calculated TRXRD profile reproduces the experimental results as shown in Fig. 3 by solid lines. The calculated echo waveforms are shown in the insets of Fig. 3. Not only the waveform deformation due to the acoustic diffraction effect but also the temporal broadening of the pulse waveform are seen, where the fitted pulse duration t_W defined by the reciprocal of peak frequency for the 1st, 20th, and 60th echo are 2.3, 7.1, and 11 ns, respectively. The waveform was determined for 140th echo traveling 130 mm.

Here, it is demonstrated that the TRTCD method is applicable to probing the roughness of optically inaccessible boundaries. The height distributions of the back surface for the polished and unpolished GaAs wafer were first measured by a laser interferometer with the spatial resolution of 0.6 μm, the result of which is shown in Fig. 4(a) with the insets of microscope images. The roughness of the unpolished surface is characterized by the standard deviation $\sigma = 0.35$ μm and the peak wavelength $a = 30$ μm of the height distribution from Fourier analysis. Figure 4(b) shows the TRXRD profile shift due to the 1st echoes for the polished (open circles) and

(a)

········ polished   —— unpolished

(b)

○ polished
▲ unpolished
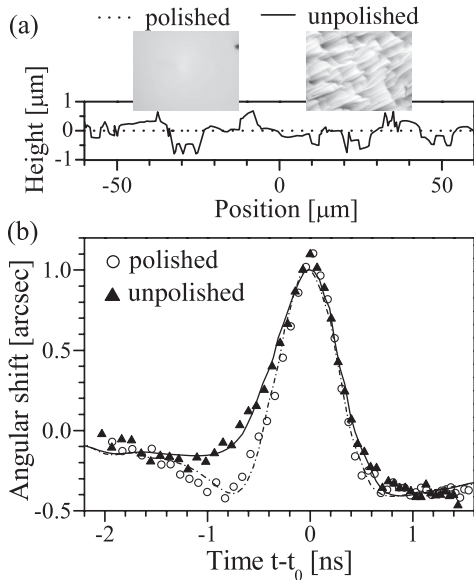
FIG. 4. (a) Height distribution of the back surface for the polished (dotted line) and unpolished (solid line) GaAs plates, measured by a laser interferometer. The standard deviation is ~ 1 nm and 0.35 μm, respectively. Insets: the microscope images 61 μm $\times$ 44 μm of the polished (left) and unpolished (right) surface. (b) The angular shift of the TRXRD profile in the part of the 1st pulse echo for the polished (open circles) and unpolished (solid triangles) GaAs plates. A broken and solid line shows the simulation curve using the Pearson VII function for the polished and unpolished plates, respectively.

unpolished (solid triangles) wafer, measured by the pump-probe method. To simulate the temporal broadening, the pulse echo waveforms were convoluted using Pearson VII function $1/(1 + \eta^2/mw^2)^m$ as a response function, where w means width and the function is reduced to Lorentzian and Gaussian for $m = 1$ and ∞, respectively. Different values of w, m, and the amplitude are used for $\eta > 0$ and < 0 in the waveform function, so that the calculated curves finely reproduce the experimental results as shown in Fig. 4(b). The pulse duration of the fitted echo waveforms are $t_W = 3.5$ and 5.9 ns for the polished and unpolished wafer, respectively. Assume that the pulse broadening of $\delta t_W = \sqrt{5.9^2 - 3.5^2}$ ns is caused by the parameter a characterizing rough structure as follows: a scatterer with size a gives rise to angle divergence $\delta \theta_d \sim \lambda/a$ for a scattered wave with wavelength λ according to Fraunhofer approximation, and the path difference due to $\delta \theta_d$ results in temporal broadening $\delta t_W \sim \delta \theta_d^2 h/2v$. Then, the pulse broadening gives $a = 60$ μm using the peak wavelength $\lambda_0 = vt_W$ (~ 17 μm) of the pulse echo for the polished wafer.

In conclusion, we have applied the TRTCD method to the detection of acoustic pulse echoes in semiconductor plates generated by ultrashort optical pulses, and obtained the surface-normal longitudinal component of a strain tensor. It has been clearly observed that the initial contrac-

tion generated a dilation-leading bipolar pulse in Si, while the dilation induced a contraction-leading pulse in GaAs. The pulse echo waveforms have been determined using a simple model considering three-dimensional wave front distortion as the phase deviation of one-dimensional elementary waves. The change in the waveforms due to the acoustic diffraction and propagation effects has been revealed. The temporal broadening of the pulse echo from a rough surface has been consistent with the roughness, which indicates the method will be applicable to the monitoring of the roughness of underlying interfaces in materials.

[1] C. Thomsen et al., Phys. Rev. Lett. **53**, 989 (1984).
[2] H. Maris, Sci. Am. **278**, No. 1, 86 (1998).
[3] V. E. Gusev and A. A. Karabutov, *Laser Optoacoustics* (American Institute of Physics, Woodbyry, NY, 1993).
[4] H. Grahn et al., IEEE J. Quantum Electron. **25**, 2562 (1989).
[5] C. J. Morath et al., Solid State Technol. **40**, 85 (1997).
[6] O. B. Wright and K. Kawashima, Phys. Rev. Lett. **69**, 1668 (1992).
[7] O. Matsuda et al., Phys. Rev. B **71**, 115330 (2005).
[8] J. R. Helliwell and P. M. Rentzepis, *Time-Resolved Diffraction* (Oxford University Press, NY, 1997).
[9] B. Adams, *Nonlinear Optics, Quantum Optics, and Ultrafast Phenomena with x-rays* (Kluwer Academic Publishers, Massachusetts, 2003).
[10] D. A. Reis et al., Phys. Rev. Lett. **86**, 3072 (2001).
[11] M. F. DeCamp et al., J. Synchrotron Radiat. **12**, 177 (2005).
[12] It is to be noted that the TRTCD technique is potentially applicable to polycrystalline materials with mosaic structure giving rise to broad x-ray rocking curves.
[13] Y. Hayashi et al., J. Synchrotron Radiat. **12**, 685 (2005).
[14] T. Hara et al., Rev. Sci. Instrum. **73**, 1125 (2002).
[15] C. Thomsen et al., Phys. Rev. B **34**, 4129 (1986).
[16] O. B. Wright and V. E. Gusev, Appl. Phys. Lett. **66**, 1190 (1995).
[17] O. B. Wright et al., Phys. Rev. B **64**, 081202 (2001).
[18] T. Ishikawa et al., Rev. Sci. Instrum. **63**, 1015 (1992).
[19] Y. Tanaka et al., Rev. Sci. Instrum. **71**, 1268 (2000).
[20] *Numerical Data and Functional Relationships in Science and Technology*, edited by O. Mandelung et al., Landlt-Bornstein, New Series, Group III (Springer, Berlin, 1982).
[21] N. C. R. Holme et al., Appl. Phys. Lett. **83**, 392 (2003).
[22] S. Takagi, Acta Crystallogr. **15**, 1311 (1962).
[23] D. Taupin, Bull. Soc. Fr. Mineral. Cristallogr. **87**, 469 (1964).
[24] C. R. Wie et al., J. Appl. Phys. **59**, 3743 (1986).